

Design and numerical evaluation of a volume coil array for parallel MR imaging at ultrahigh fields

Yong Pang¹, Ernest W.H. Wong², Baiying Yu³, Xiaoliang Zhang^{1,4,5}

¹Department of Radiology and Biomedical Imaging, University of California San Francisco, San Francisco, CA, USA; ²Agilent Technologies, Santa Clara, CA, USA; ³Magwale, Palo Alto, CA, USA; ⁴UC Berkeley/UCSF Joint Graduate Group in Bioengineering, San Francisco & Berkeley, CA, USA; ⁵California Institute for Quantitative Biosciences (QB3), San Francisco, CA, USA

Corresponding to: Xiaoliang Zhang, PhD. Department of Radiology and Biomedical Imaging, University of California San Francisco, Byers Hall, Room 102D, 1700 4th ST, San Francisco, CA 94158-2330, USA. Email: xiaoliang.zhang@ucsf.edu.

Abstract: In this work, we propose and investigate a volume coil array design method using different types of birdcage coils for MR imaging. Unlike the conventional radiofrequency (RF) coil arrays of which the array elements are surface coils, the proposed volume coil array consists of a set of independent volume coils including a conventional birdcage coil, a transverse birdcage coil, and a helix birdcage coil. The magnetic fluxes of these three birdcage coils are intrinsically cancelled, yielding a highly decoupled volume coil array. In contrast to conventional non-array type volume coils, the volume coil array would be beneficial in improving MR signal-to-noise ratio (SNR) and also gain the capability of implementing parallel imaging. The volume coil array is evaluated at the ultrahigh field of 7T using FDTD numerical simulations, and the g-factor map at different acceleration rates was also calculated to investigate its parallel imaging performance.

Keywords: Volume coil array; birdcage coil; transverse birdcage coil; helix birdcage coil; signal-to-noise ratio (SNR); g-factor map; parallel imaging



Submitted Jan 15, 2014. Accepted for publication Feb 26, 2014.

doi: 10.3978/j.issn.2223-4292.2014.02.07

Scan to your mobile device or view this article at: <http://www.amepc.org/qims/article/view/3438/4292>

Introduction

Radiofrequency (RF) coil arrays with a set of surface coils (1-7) become more popular in MR imaging as they can provide improved signal-to-noise ratio and the capability of performing parallel imaging (8-30). Compared with surface coils, RF volume coils, such as birdcage coils (31), are able to generate homogenous magnetic fields (B_1) and potentially uniform MR images (17,32-36,37-53). In recent years it has been demonstrated that multiple tuned volume coils for multiple nuclear MR applications (54) can be designed by integrating different type of birdcage coils which are intrinsically decoupled due to the cancellation of their magnetic flux. In this work, we propose and investigate a single tuned proton volume coil array based on that design concept using combination of different typed birdcage coils for improving SNR (31) and also for implementing parallel imaging (55-59) and parallel transmission (60-65) to accelerate imaging. To demonstrate the design concept, a

3-channel volume coil array was designed, which consists of a conventional birdcage coil, a transverse birdcage coil, and a helix birdcage coil. All the three coils were intrinsically decoupled and tuned to 298 MHz which is corresponding to proton frequency at 7T. By taking advantage of the intrinsic decoupling feature, this volume coil array can be designed without using any decoupling circuitry between array elements. The performance of the volume coil array is evaluated using FDTD numerical simulation (39,66-69) in terms of the RF field distribution and mutual coupling. The parallel imaging performance of the 3-element volume coil array was also evaluated by calculating the g-factor map (56) at different acceleration rates for SENSE reconstruction.

Methods

The structure of the proposed multichannel volume coil array is shown in *Figure 1*. The inner coil is a 16-strut low-

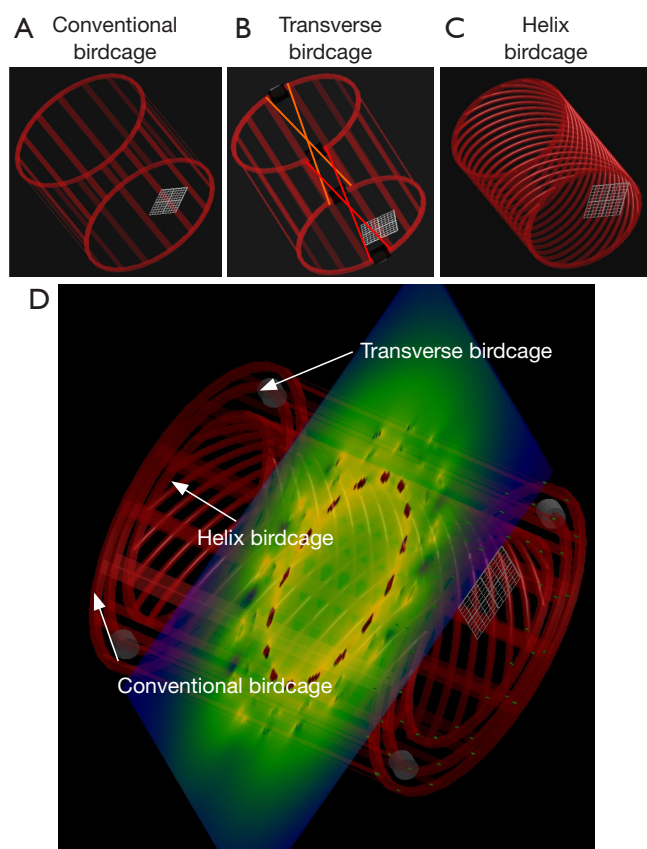


Figure 1 The 3-channel volume coil array consists of 3 different birdcage coils: (A) Conventional birdcage coil (outer); (B) Transverse Birdcage coil (middle); and (C) Helix birdcage coil (inner); (D) The volume coil array.

pass helix birdcage coil with 3 cm ID, the middle coil is a 16-strut birdcage coil with 3.8 cm ID, while the outer coil is a conventional birdcage coil with 4.5 cm ID. The coils were all built using copper tape and the coil length was 4 cm. Capacitors were placed on each strut and used to tune the resonant frequency to 298 MHz. The coaxial feed port was modeled as a voltage source with 50 Ohm impedance. The software XFDTD6.4 (Remcom Inc., State College, PA, USA) was used to model this 3-channel birdcage coil array and evaluate the magnetic field distribution. The Yee cell size was 0.5 mm on both the transverse plane and longitudinal direction which was small enough for satisfying the accuracy requirement of the FDTD calculation. The boundary condition was set as Perfectly Matching Layers (PML). To ensure the calculation stability and accurate performance of the PML absorbing boundaries, in each direction 20 Yee cells of free space padding were placed

between the PML boundary and the conducting materials. The Gauss waveform was used to sweep frequency to determine the proper capacitance value for each volume coil working at 298.2 MHz, and the stop criteria were that the calculation converged to -30 dB. Then, after obtaining the capacitance, the sinusoid waveform was used to calculate the RF field distributions and the stop criteria were set as the calculation converged to -30 dB.

To demonstrate the parallel imaging performance of the proposed 3-element volume coil array, the g -factor maps at different acceleration rates were calculated and plotted based on the RF field distribution calculated from the FDTD simulation by using the equation below (56):

$$g_{\rho} = \sqrt{\frac{1}{(S^H \Psi^{-1} S)^{-1}} \Big|_{\rho, \rho} (S^H \Psi^{-1} S)_{\rho, \rho}} \quad [1]$$

where ρ is the index of voxel in the FOV, S is the reduced Fourier encoding, Ψ is the noise correlation matrix between channels. The g -factor is strongly dependent on the voxel position and is related to the signal to noise ratio (SNR):

$$SNR_{\rho}^{red} = \frac{SNR_{\rho}^{full}}{g_{\rho} \sqrt{R}} \quad [2]$$

where R is the acceleration rate, showing that the SNR of the accelerated image is inversely proportional to the g -factor.

Results

The simulated B_1 field distribution is shown in *Figure 2*. The 1st row is the results of the conventional birdcage; the 2nd row is the results of the transverse birdcage coil, while the 3rd row is the helix birdcage coil. The left column results are the B_1 field distribution of each coil when combined together as a birdcage coil array, while the right column results are the B_1 distribution of each individual coil. It is clearly shown that, the B_1 field distribution of each birdcage coil within the volume coil is almost the same as that of the individual coil, demonstrating excellent isolation between the three channels. The blue arrows in the figures denote the direction of the magnetic field flux density. In a conventional birdcage coil, the B_1 directions are along one direction within the whole coil; in a transverse birdcage coil, the B_1 directions of the two halves are opposed to each other; while in the helix birdcage coil, the B_1 direction in one slice is the same, but along the longitudinal direction the B_1 direction varies from 0° to 360° , therefore its net magnetic flux is zero. Thus the flux from one coil to the others is theoretically zero, leading to excellent decoupling between

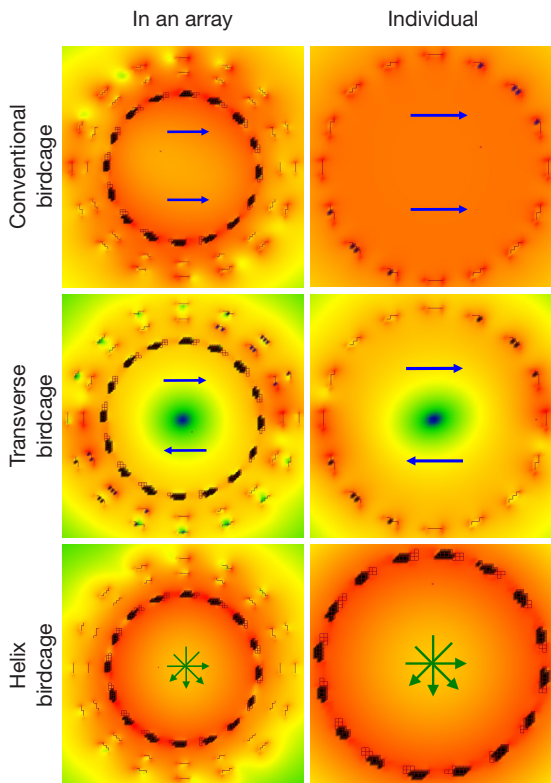


Figure 2 Left column, B_1 pattern of each volume coil when put in the 3-channel birdcage coil array; Right column, B_1 pattern of each individual volume coil when stand alone. 1st row, The B_1 pattern of the conventional birdcage coil; 2nd row, B_1 pattern of the transverse birdcage coil; 3rd row, B_1 pattern of the helix birdcage coil. The B_1 pattern of the birdcage coil in the array is the same as that of an individual coil with same type, demonstrating the excellent decoupling performance between the 3 birdcage coils within the 3-channel birdcage coil array. The blue arrow denotes the magnetic flux direction in the birdcage coils. The green arrows in the Helix birdcage coil denote that the magnetic flux direction in transverse plane are identical, but varies along the longitudinal axis, therefore the net flux is zero.

each pair of birdcage coils.

Figure 3 shows the sensitivity maps and phase maps on transverse plane of the three volume coil elements when fed individually. This transverse plane is the central slice. Each element shows different B_1 distribution, leading to different sensitivity maps which can be used for parallel imaging. Figure 4 shows the g-factor maps for 1D SENSE reconstruction at different acceleration rates: R = 1.2, 1.5, 1.7, 2.0, 2.3 and 2.5. The acceleration rate and the corresponding

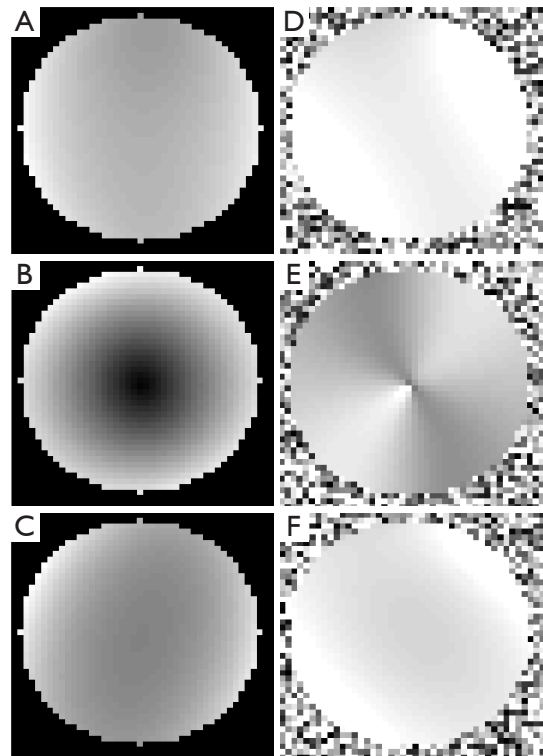


Figure 3 The transverse sensitivity maps of each array element at the central slice: (A) Conventional birdcage coil; (B) Transverse birdcage coil; (C) Helix birdcage coil. The phase maps of the B_1 field of each array element: (D) Conventional birdcage coil; (E) Transverse birdcage coil; (F) Helix birdcage coil.

average g-factor are shown on the top of each g-map. It is demonstrated that with the increase of the acceleration the average g-factor increases (Figure 5). At acceleration rate of 2, the g-factor is around 1.5, which is practically good for performing parallel imaging for this 3-element coil array.

Discussion and conclusions

In this work, a novel volume coil array design using different types of birdcage coils is proposed for MR imaging. The resonant elements of this volume coil array are a conventional birdcage coil, a transverse birdcage coil and a helix birdcage coil. The field behavior and the parallel imaging performance of the volume coil array have been investigated using numerical simulations and SENSE parallel imaging algorithm. The studies verify the theoretical expectation on electromagnetic decoupling performance of these birdcage coil elements, demonstrating

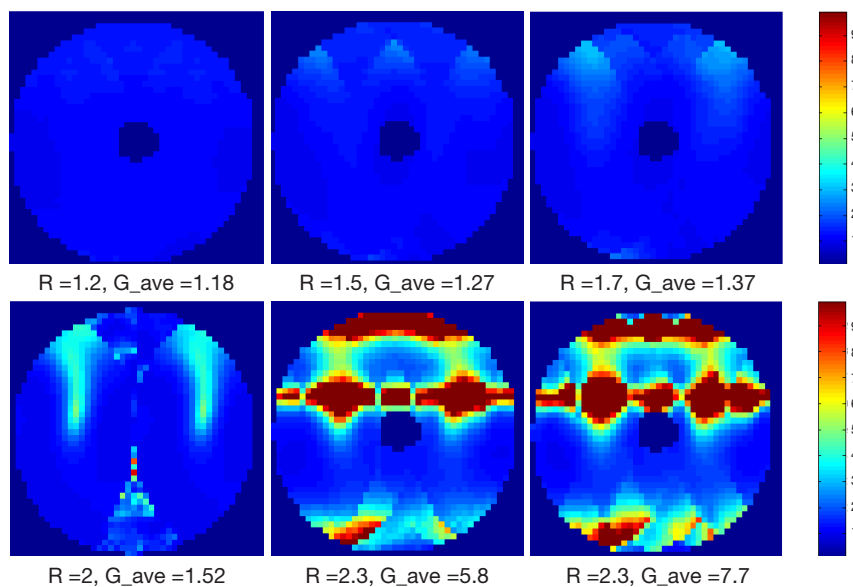


Figure 4 G-factor maps for 1D SENSE reconstruction at acceleration rate $R=1.2, 1.5, 1.7, 2, 2.3$ and 2.5 . At reduction factor of 2, the g-factor is approximately 1.5, which is adequate for this 3-element coil array.

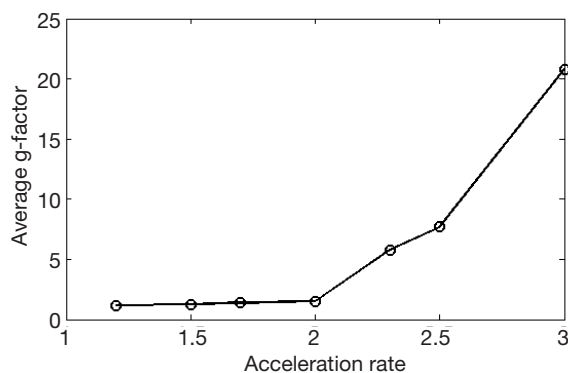


Figure 5 The average g-factor varies with the acceleration rate from (1.2 to 3).

the feasibility of this volume coil array design technique. From the results it can be seen that the three birdcage coils are deeply decoupled from each other due to their unique magnetic flux directions resulting in the net magnetic flux cancellation in both the transverse birdcage coil and the helix birdcage coil. In this design method with intrinsic decoupling feature, there is no dedicated decoupling circuits needed, making the volume coil array design simple and practical. Each element of a volume coil array has bigger imaging coverage than that of conventional surface coil arrays, which may potentially lead to a better g-factor and ultimately improved parallel imaging performance,

particularly in imaging with large field-of-view (FOV). Compared with conventional non-array volume coils, the volume coil array is expected to provide increased SNR in MR imaging. Typical magnetic field distribution of surface coil arrays is not uniform over the FOV, showing strong gradient behavior with much higher signal intensity in the peripheral area and weak signal in the center region. With the volume coil array, more uniform SNR distribution can be expected across a large volume.

Acknowledgements

This work was partially supported by NIH grants EB004453, EB008699, K99EB015487 and P41EB013598, a QB3 Research Award, a Springer Med Fund Award, and a National Natural Science Foundation of China Grant (51228702).

Disclosure: The authors declare no conflict of interest.

References

1. Ackerman JJ, Grove TH, Wong GG, et al. Mapping of metabolites in whole animals by ^{31}P NMR using surface coils. *Nature* 1980;283:167-70.
2. Roemer PB, Edelstein WA, Hayes CE, et al. The NMR phased array. *Magn Reson Med* 1990;16:192-225.
3. Hayes CE, Tsuruda JS, Mathis CM. Temporal lobes:

- surface MR coil phased-array imaging. *Radiology* 1993;189:918-20.
4. Porter JR, Wright SM, Reykowski A. A 16-element phased-array head coil. *Magn Reson Med* 1998;40:272-9.
 5. Zhang X, Ugurbil K, Chen W. Microstrip RF surface coil design for extremely high-field MRI and spectroscopy. *Magn Reson Med* 2001;46:443-50.
 6. Weiger M, Pruessmann KP, Leussler C, et al. Specific coil design for SENSE: a six-element cardiac array. *Magn Reson Med* 2001;45:495-504.
 7. Wiggins GC, Triantafyllou C, Potthast A, et al. 32-channel 3 Tesla receive-only phased-array head coil with soccer-ball element geometry. *Magn Reson Med* 2006;56:216-23.
 8. Balu N, Yarnykh VL, Scholnick J, et al. Improvements in carotid plaque imaging using a new eight-element phased array coil at 3T. *J Magn Reson Imaging* 2009;30:1209-14.
 9. Wright SM, McDougall MP, Brown DG. Single Echo Acquisition (SEA) MR Imaging. *Proceedings of International Society of Magnetic Resonance in Medicine, Toronto, Canada, 2003:23.*
 10. Buehrer M, Pruessmann KP, Boesiger P, et al. Array compression for MRI with large coil arrays. *Magn Reson Med* 2007;57:1131-9.
 11. Chang G, Friedrich KM, Wang L, et al. MRI of the wrist at 7 tesla using an eight-channel array coil combined with parallel imaging: preliminary results. *J Magn Reson Imaging* 2010;31:740-6.
 12. Hardy CJ, Cline HE, Giaquinto RO, et al. 32-element receiver-coil array for cardiac imaging. *Magn Reson Med* 2006;55:1142-9.
 13. Hardy CJ, Giaquinto RO, Piel JE, et al. 128-channel body MRI with a flexible high-density receiver-coil array. *J Magn Reson Imaging* 2008;28:1219-25.
 14. Henry RG, Fischbein NJ, Dillon WP, et al. High-sensitivity coil array for head and neck imaging: technical note. *AJNR Am J Neuroradiol* 2001;22:1881-6.
 15. Lee RF, Hardy CJ, Sodickson DK, et al. Lumped-element planar strip array (LPSA) for parallel MRI. *Magn Reson Med* 2004;51:172-83.
 16. Adriany G, Van de Moortele PF, Wiesinger F, et al. Transmit and receive transmission line arrays for 7 Tesla parallel imaging. *Magn Reson Med* 2005;53:434-45.
 17. Wiggins GC, Potthast A, Triantafyllou C, et al. Eight-channel phased array coil and detunable TEM volume coil for 7 T brain imaging. *Magn Reson Med* 2005;54:235-40.
 18. Zhu Y, Hardy CJ, Sodickson DK, et al. Highly parallel volumetric imaging with a 32-element RF coil array. *Magn Reson Med* 2004;52:869-77.
 19. Li Y, Xie Z, Pang Y, et al. ICE decoupling technique for RF coil array designs. *Med Phys* 2011;38:4086-93.
 20. Boskamp EB, Lee RF. Whole body LPSA transceiver array with optimized transmit homogeneity. *Proceedings of International Society of Magnetic Resonance in Medicine, Honolulu, HI, 2002:903.*
 21. Pang Y, Zhang X, Xie Z, et al. Common-mode differential-mode (CMDM) method for double-nuclear MR signal excitation and reception at ultrahigh fields. *IEEE Trans Med Imaging* 2011;30:1965-73.
 22. Wu B, Wang C, Krug R, et al. 7T human spine imaging arrays with adjustable inductive decoupling. *IEEE Trans Biomed Eng* 2010;57:397-403.
 23. Wu B, Wang C, Kelley DA, et al. Shielded microstrip array for 7T human MR imaging. *IEEE Trans Med Imaging* 2010;29:179-84.
 24. Wu B, Li Y, Wang C, et al. Multi-reception strategy with improved SNR for multichannel MR imaging. *PLoS One* 2012;7:e42237.
 25. Wu B, Wang C, Lu J, et al. Multi-channel microstrip transceiver arrays using harmonics for high field MR imaging in humans. *IEEE Trans Med Imaging* 2012;31:183-91.
 26. Wu B, Zhang X, Wang C, et al. Flexible transceiver array for ultrahigh field human MR imaging. *Magn Reson Med* 2012;68:1332-8.
 27. Li Y, Yu B, Pang Y, et al. Planar quadrature RF transceiver design using common-mode differential-mode (CMDM) transmission line method for 7T MR imaging. *PLoS One* 2013;8:e80428.
 28. Li Y, Pang Y, Vigneron D, et al. Investigation of multichannel phased array performance for fetal MR imaging on 1.5T clinical MR system. *Quant Imaging Med Surg* 2011;1:24-30.
 29. Pang Y, Zhang X. Precompensation for mutual coupling between array elements in parallel excitation. *Quant Imaging Med Surg* 2011;1:4-10.
 30. Gilbert KM, Belliveau JG, Curtis AT, et al. A conformal transceiver array for 7 T neuroimaging. *Magn Reson Med* 2012;67:1487-96.
 31. Hayes C, Edelstein W, Schenck J, et al. An efficient, highly homogeneous radiofrequency coil for whole-body NMR imaging at 1.5T. *J Magn Reson* 1985;63:622-8.
 32. Alecci M, Collins CM, Smith MB, et al. Radio frequency magnetic field mapping of a 3 Tesla birdcage coil: experimental and theoretical dependence on sample properties. *Magn Reson Med* 2001;46:379-85.
 33. Avdievich NI, Hetherington HP. 4 T Actively detuneable

- double-tuned $^1\text{H}/^{31}\text{P}$ head volume coil and four-channel ^{31}P phased array for human brain spectroscopy. *J Magn Reson* 2007;186:341-6.
34. Vaughan JT, Adriany G, Garwood M, et al. Detunable transverse electromagnetic (TEM) volume coil for high-field NMR. *Magn Reson Med* 2002;47:990-1000.
 35. Vaughan JT, Hetherington HP, Otu JO, et al. High frequency volume coils for clinical NMR imaging and spectroscopy. *Magn Reson Med* 1994;32:206-18.
 36. Wen H, Chesnick AS, Balaban RS. The design and test of a new volume coil for high field imaging. *Magn Reson Med* 1994;32:492-8.
 37. Zhang X, Ugurbil K, Chen W. A microstrip transmission line volume coil for human head MR imaging at 4T. *J Magn Reson* 2003;161:242-51.
 38. Fujita H, Braum WO, Morich MA. Novel quadrature birdcage coil for a vertical B(0) field open MRI system. *Magn Reson Med* 2000;44:633-40.
 39. Ibrahim TS, Lee R, Baertlein BA, et al. B1 field homogeneity and SAR calculations for the birdcage coil. *Phys Med Biol* 2001;46:609-19.
 40. Jin J, Shen G, Perkins T. On the field inhomogeneity of a birdcage coil. *Magn Reson Med* 1994;32:418-22.
 41. Lin FH, Kwong KK, Huang IJ, et al. Degenerate mode birdcage volume coil for sensitivity-encoded imaging. *Magn Reson Med* 2003;50:1107-11.
 42. Murphy-Boesch J, Srinivasan R, Carvajal L, et al. Two configurations of the four-ring birdcage coil for ^1H imaging and ^1H -decoupled ^{31}P spectroscopy of the human head. *J Magn Reson B* 1994;103:103-14.
 43. Shen GX, Boada FE, Thulborn KR. Dual-frequency, dual-quadrature, birdcage RF coil design with identical B1 pattern for sodium and proton imaging of the human brain at 1.5 T. *Magn Reson Med* 1997;38:717-25.
 44. Tropp J. The theory of the birdcage resonator. *J Magn Reson* 1989;82:51-62.
 45. Vullo T, Zipagan RT, Pascone R, et al. Experimental design and fabrication of birdcage resonators for magnetic resonance imaging. *Magn Reson Med* 1992;24:243-52.
 46. Wang C, Qu P, Shen GX. Potential advantage of higher-order modes of birdcage coil for parallel imaging. *J Magn Reson* 2006;182:160-7.
 47. Zhang X, Ugurbil K, Sainati R, et al. An inverted-microstrip resonator for human head proton MR imaging at 7 tesla. *IEEE Trans Biomed Eng* 2005;52:495-504.
 48. Pang Y, Xie Z, Li Y, et al. Resonant Mode Reduction in Radiofrequency Volume Coils for Ultrahigh Field Magnetic Resonance Imaging. *Materials (Basel)* 2011;4:1333-44.
 49. Wang C, Li Y, Wu B, et al. A practical multinuclear transceiver volume coil for in vivo MRI/MRS at 7 T. *Magn Reson Imaging* 2012;30:78-84.
 50. Pang Y, Xie Z, Xu D, et al. A dual-tuned quadrature volume coil with mixed $\lambda/2$ and $\lambda/4$ microstrip resonators for multinuclear MRSI at 7 T. *Magn Reson Imaging* 2012;30:290-8.
 51. Zhang X, Zhu XH, Chen W. Higher-order harmonic transmission-line RF coil design for MR applications. *Magn Reson Med* 2005;53:1234-9.
 52. Alsop DC, Connick TJ, Mizsei G. A spiral volume coil for improved RF field homogeneity at high static magnetic field strength. *Magn Reson Med* 1998;40:49-54.
 53. Li Y, Wang C, Yu B, et al. Image homogenization using pre-emphasis method for high field MRI. *Quant Imaging Med Surg* 2013;3:217-23.
 54. Wong WH, Unno S, Anderson WA. Multiple tuned birdcage coils. United States of America, 2002, Patent No. US6420871.
 55. Sodickson DK, Manning WJ. Simultaneous acquisition of spatial harmonics (SMASH): fast imaging with radiofrequency coil arrays. *Magn Reson Med* 1997;38:591-603.
 56. Pruessmann KP, Weiger M, Scheidegger MB, et al. SENSE: sensitivity encoding for fast MRI. *Magn Reson Med* 1999;42:952-62.
 57. Griswold MA, Jakob PM, Heidemann RM, et al. Generalized autocalibrating partially parallel acquisitions (GRAPPA). *Magn Reson Med* 2002;47:1202-10.
 58. Ji JX, Son JB, Rane SD. PULSAR: a matlab toolbox for parallel magnetic resonance imaging using array coils and multiple channel receivers. *Concepts Magn Reson B: Magn Reson Eng* 2007;31B:24-36.
 59. Lin FH, Kwong KK, Belliveau JW, et al. Parallel imaging reconstruction using automatic regularization. *Magn Reson Med* 2004;51:559-67.
 60. Katscher U, Börnert P, Leussler C, et al. Transmit SENSE. *Magn Reson Med* 2003;49:144-50.
 61. Zhu Y. Parallel excitation with an array of transmit coils. *Magn Reson Med* 2004;51:775-84.
 62. Grissom W, Yip CY, Zhang Z, et al. Spatial domain method for the design of RF pulses in multicoil parallel excitation. *Magn Reson Med* 2006;56:620-9.
 63. Ma C, Xu D, King KF, et al. Joint design of spoke trajectories and RF pulses for parallel excitation. *Magn Reson Med* 2011;65:973-85.
 64. Xu D, King KF, Liang ZP. Improving k-t SENSE by

- adaptive regularization. *Magn Reson Med* 2007;57:918-30.
65. Zhang X, Pang Y. Parallel Excitation in Ultrahigh Field Human MR Imaging and Multi-Channel Transmit System. *OMICS J Radiol* 2012;1:e110.
66. Collins CM, Yang QX, Wang JH, et al. Different excitation and reception distributions with a single-loop transmit-receive surface coil near a head-sized spherical phantom at 300 MHz. *Magn Reson Med* 2002;47:1026-8.
67. Yang QX, Wang J, Zhang X, et al. Analysis of wave behavior in lossy dielectric samples at high field. *Magn Reson Med* 2002;47:982-9.
68. Wang J, Yang QX, Zhang X, et al. Polarization of the RF field in a human head at high field: a study with a quadrature surface coil at 7.0 T. *Magn Reson Med* 2002;48:362-9.
69. Pang Y, Wu B, Wang C, et al. Numerical Analysis of Human Sample Effect on RF Penetration and Liver MR Imaging at Ultrahigh Field. *Concepts Magn Reson Part B Magn Reson Eng* 2011;39B:206-16.

Cite this article as: Pang Y, Wong EWH, Yu B, Zhang X. Design and numerical evaluation of a volume coil array for parallel MR imaging at ultrahigh fields. *Quant Imaging Med Surg* 2014;4(1):50-56. doi: 10.3978/j.issn.2223-4292.2014.02.07